Chen et al. PhotoniX (2021) 2:2
https://doi.org/10.1186/s43074-021-00024-2

PhotoniX

REVIEW Open Access

Optical waveguides based on one-dimensional organic crystals

Song Chen[1], Ming-Peng Zhuo[1], Xue-Dong Wang[1], Guo-Qing Wei[1] and Liang-Sheng Liao[1,2*]

* Correspondence: lsliao@suda.edu.cn
[1]Jiangsu Key Laboratory for Carbon-Based Functional Materials & Devices, Institute of Functional Nano & Soft Materials (FUNSOM), Soochow University, Suzhou, Jiangsu 215123, People's Republic of China
[2]Institute of Organic Optoelectronics, JITRI, Wujiang, Suzhou, Jiangsu 215211, People's Republic of China

Abstract

Optical waveguide of organic micro/nanocrystals is one of crucial elements in miniaturized integrated photonics. One-dimensional (1D) organic crystals with various optical features have attracted increasing interests towards promising photonic devices, such as multichannel signal converter, organic field-effect optical waveguide, sensitive detector, and optical logic gate. Therefore, a summary about the 1D organic micro/nanocrystals based optical waveguide is important for the rational design and fabrication of novel optical devices towards optoelectronics applications. Herein, recent advances of optical waveguide based on 1D organic micro/nanocrystals with solid, flexible, hollow, uniformly doped, core-shell, multiblock and branched structures are summarized from the aspects of the waveguide properties and applications in photonic devices. Furthermore, we presented our personal view about the expectation of future development in 1D organic optical waveguide for the photonic applications.

Keywords: Organic semiconductor molecules, Self-assembly, Organic micro/nanostructures, Optical waveguide, Organic photonics

Introduction

Optical waveguide, with light transmitting internally by total reflection at the interface of an optical medium, is a crucial element in many miniaturized integrated nanophotonics devices. Prof. Kao K, the father of optical fiber communications, was awarded the Nobel Prize 2009 in physics to praise his contribution in the transmission of light in fibers for optical communication. His achievements started a new era of human technology in information interaction. Up to date, micro/nanoscale optical waveguide based on various solid-state materials is one of the essential components to guide light. Remarkably, organic semiconductor materials with the excellent optoelectronic performance [1] have been proved to be promising candidates as the building blocks of photonic devices. Specifically, one-dimensional (1D) organic semiconductor crystals are generally suitable for the transport of photons, electrons, and excitons. Moreover, the 1D crystal with π-conjugated organic molecules can enhance charge-transporting mobility [2, 3]. These materials possess fundamental advantages including tailoring capability [4], good processability [5], few defects [2], uniform morphology [6], good thermal stability [7], solution processing [8] and high photoluminescence (PL)

efficiency [9–11]. These organic molecular materials typically have weak intermolecular interactions between molecules, including hydrogen bonds, halogen bonds, π-π interactions, and van der Waals interactions. Optical properties of these organic molecules not only can be tuned via adjusting their molecular structures and packing mode, but also can be modified by a rational doping strategy. Therefore, these features allow such 1D crystals being used as "efficient optical waveguide" materials to significantly improve the wave propagation in media.

Additionally, the self-assembled 1D crystals from organic emissive molecules exhibit extensive optical-related applications, such as organic field-effect transistors (OFETs) [12–15], organic light-emitting transistors (OLETs) [16], chemical sensors [8, 17] and tunable color displays [18–20], which serve as the effective building blocks for organic integrated photonics. The photon propagation in the organic crystals has two different ways. The active optical waveguide refers to the optical output from the intrinsic emission of the sample by exciting it with an external energy source, whereas the passive optical waveguide mode refers to the light propagation of optical source [21–25]. But the single crystals cannot transport the multi-waveguide mode [26]. To address this issue, researchers pay more attention to multi-level micro/nanostructure. The organic heterostructures demonstrate the superior physicochemical features and the mixed passive/active waveguide mode, which is favorable for the development of multifunctional optoelectronic devices in the future. As is shown in Fig. 1d crystals have various morphologies including solid state, flexible, electrically controlled, hollow, uniformly doped, core/shell, multiblock, and branched structure. And their applications are illustrated in Fig. 2, including OFET, optical waveguide modulator, multichannel signal

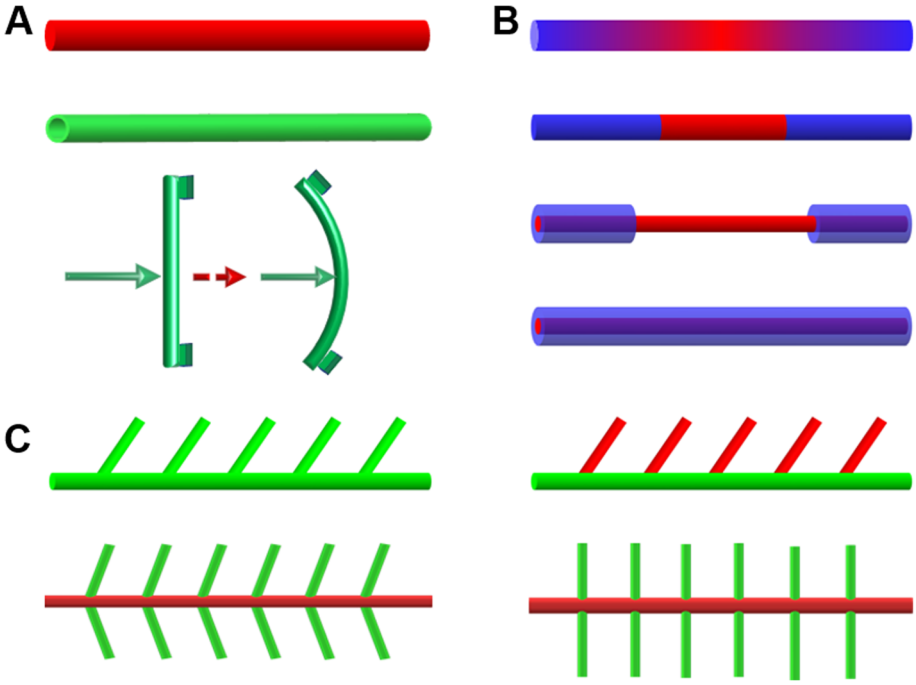

Fig. 1 Various 1D organic crystal structures. **a** Schematic diagram of 1D organic the single component microcrystals. **b** Schematic illustration of 1D organic multi-component horizontal microcrystals. **c** Graphic expression of 1D organic single/multi-component branched microcrystals

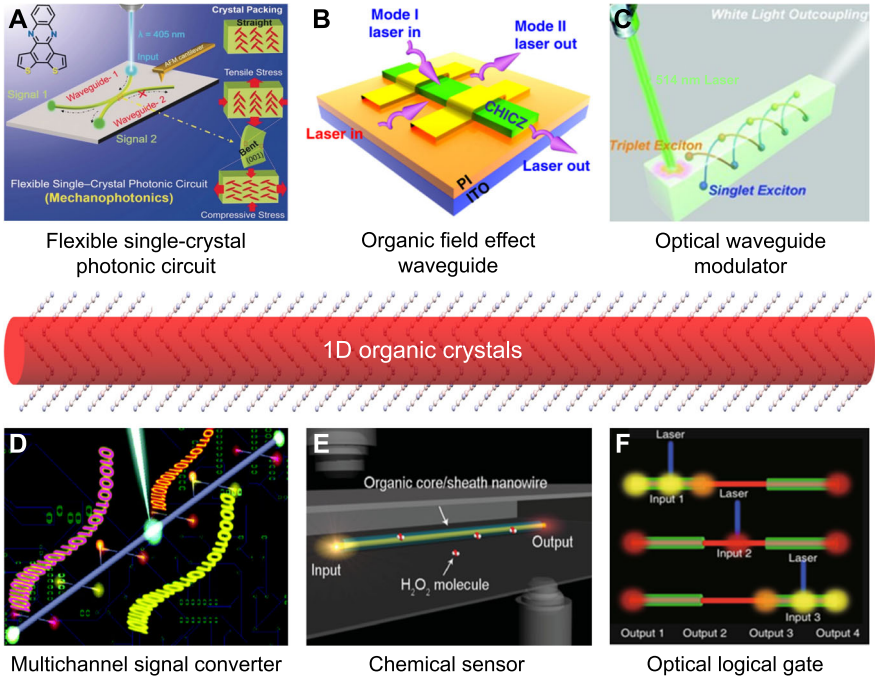

Fig. 2 1D organic crystals: organic photonics. **a** Reprinted with permission from ref. [27] Copyright 2020, Wiley-VCH. **b** Reprinted with permission from ref. [28] Copyright 2018, Nature Publishing Group. C Reprinted with permission from ref. [29] Copyright 2011, Wiley-VCH. D Reprinted with permission from ref. [30] Copyright 2012, American Chemical Society. E Reprinted with permission from ref. [31] Copyright 2012, Wiley-VCH. F Reprinted with permission from ref. [32] Copyright 2019, Nature Publishing Group

converter, chemical sensor, optical logical gate and optical router. Table 1 also lists the representative examples of optical waveguides, elaborating the materials, crystal morphologies, emission colors and waveguide performances. In this review, after introducing the fundamentals of optical waveguides, we will focus on recent advances in optical waveguides of 1D crystals with various morphologies at micro/nanoscale as well as their diverse optoelectronic performance. Then we will discuss the challenges remained and provide our perspectives in this field.

The fundamental mechanism of optical waveguide

Optical waveguide is an optical medium for wave transmission [1], which has attracted more and more researcher's attention. In this part, the optical waveguide of 1D micro/nanostructures based on organic small molecules is mainly described. Two factors are required to form an optical waveguide: one is a medium with a higher refractive index than that of the external environment [2], the other is total internal reflection. The optical waveguide mechanism is illustrated in Fig. 3a [49], where the transparent medium n_1 has higher refractive index than that of the environment (n_2 and n). The total internal reflection occurs when the light propagates from the denser medium (n_1) to the less dense medium (n_2 or n) and the incident angle θ_1 is greater than the critical angle (the formula is $\theta_c = \arcsin(n_2/n_1)$). Thereby, the optical field can be well-confined in 1D micro/nanostructures (Fig. 3b) [51].

As we have already known, organic crystals based on small organic molecules have outstanding crystallinity and elimination of crystal boundaries, which is beneficial to

Table 1 Representative examples of organic optical waveguides

Morphology	Materials	Emission Colors	Loss Coefficient (dB/μm)	Refs
Microrod	Perylene diimide (PDI)	Red	0.13	[33]
	Diphenylalanine (FF)	White		[34]
	9,10-bis (phenylethynyl) anthracene (BPEA)	Orange		[35]
Microribbon	2,8-dichloro-5,11-dihexyl-indolo(3,2-b) carbazole (CHICZ)	Blue	0.01	[28]
	1,4-bis((*E*)-4-(1,2,2-triphenylvinyl)-styryl)-2,5-dimethoxybenzene (TPDSB)	Green	0.0175	[36]
1D flexible microstructure	Tetrafluoropyridyl derivative 1	Orange	$R_{bending} = 0.00047$, $R_{straight} = 0.00043$	[37]
	Pentafluorophenyl derivative 2	Green	$R_{bending} = 0.001003$, $R_{straight} = 0.000703$	[37]
	(E)-1-(4-(dimethylamino)phenyl)iminomethyl-2-hydroxyl-naphthalene (DPIN)	red	$R_{bending} = 0.000274$, $R_{straight} = 0.000270$	[38]
	1,4-bis(2-cyanophenylethynyl)benzene	Blue	$R_{straight} = 0.4967$	[39]
1D microtube	9,10-bis (phenylethynyl) anthracene (BPEA)	Yellow		[40]
	Polydiacetylene (PDA)	Red	0.18	[41]
	Cocrystal: 4,4′-((1*E*,1′*E*) - (2,5-dimethoxy-1,4-phenylene) bis (ethene-2,1-diyl)) dipyridine (DPEpe) and 1,4-diiodotetrafluorobenzene (F_4DIB)	Green	0.0145	[42]
1D uniformly doped microtube	Perylene doped 2,4,5-triphenylimidazole (TPI)	UV/green	0.097	[43]
1D uniformly doped microwire	Iridium (III) bis (2-phenyl benzothiozolato-N, C2′) acetylacetonate ($(BT)_2$Ir(acac) doped 9,10-diphenylanthracene (DPA)	Yellow	0.13	[29]
	Perylene doped TPI	UV/green	0.155	[43]
1D core/shell microrod	9,10-bis (phenylethynyl) anthracene (BPEA)/ chemo-reactive bis(2,4,5-trichloro-6-carbopentoxy-phenyl) oxalate (CPPO)	Yellow/ green		[31]
	4,4′-((1*E*,1′*E*) - (2,5-dimethoxy-1,4-phenylene) bis (ethene-2,1-diyl)) dipyridine (DPEpe)/DPEpe -HCl	Green/red	0.0338	[44]
	DPEpe-HCl/DPEpe	Red/green	0.054	[44]
	Cocrystal: DPEpe and 4-bromo-2,3,5,6-tetra-fluorobenzoic acid (BrFTA)/DPEpe and 1,4-diiodotetra-fluorobenzene (F_4DIB)	Red/yellow		[32]
1D multiblock microstructure	*trans*-2,2′-((1*E*,1′*E*)-1,4-phenylenebis (ethene-2,1-diyl))-dibenzonitrile (*trans-o*-BCB)/ *Cis*-2,2′-((1*E*,1′*E*)-1,4-phenylenebis (ethene-2,1-diyl))-dibenzonitrile (*Cis-o*-BCB)	Blue/red	0.035	[45]
	$[Ru(bpy)_3]^{2+}$ (bpy = 2,2′-bipyridine) doped $[Ir(ppy)_2(pzpy)]^{+}$ (ppy = 2 phenyl pyridine, pzpy = 2-(1H-pyrazol-1-yl) pyridine)	Green/red/ orange		[46]
	Closed-state (L-c)	Blue		[22]
	Open-state (L-o)	Blue		[22]
1D branched microstructure	Aluminum tris(8-Hydroxyquinoline) (Alq_3) and 1,5-diaminoanthraquinone (DAAQ)	Red/green		[30]
	1,4-dimethoxy-2,5-di[4′-(cyano) styryl] benzene (COPV) and 2,4,5 triphenyl imidazole (TPI)	Blue/green		[47]
	2,2′-((1*E*,1′*E*)-1,4-phenylenebis (ethene-2,1-diyl))-dibenzonitrile (*o*-BCB)	Green		[48]

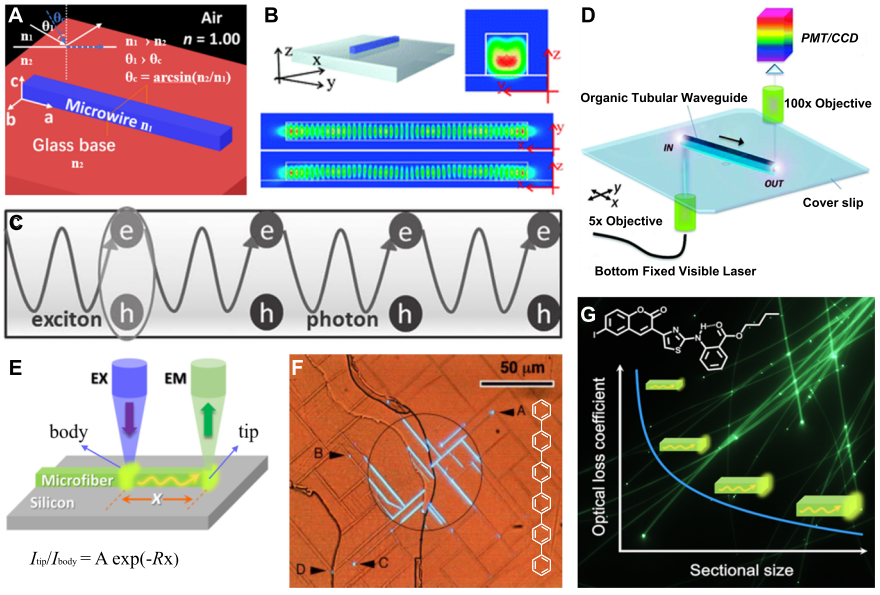

Fig. 3 The mechanism of one-dimensional waveguide and its influencing factors and test method. **a** Illustration of the theory of 1D optical waveguide. **b** Simulated 1D electric-field intensity distribution within a microwire. **c** Illustration of the formation of exciton polaritons, resulting from the strong coupling of photons and excitons. **d** Schematic demonstration of the experimental setup for the optical characterization. **e** Schematic demonstration of waveguide loss formula. **f** Fluorescence micrograph of the needlelike *p*-6P crystals. Scale bar: 50 μm. **g** Plot of optical loss coefficient versus sectional size of microfibers and exponential fit (bule line). **a, e, g** Reprinted with permission from ref. [49] Copyright 2019, American Chemical Society. **b, c** Reprinted with permission from ref. [50] Copyright 2014, Wiley-VCH. **d** Reprinted with permission from ref. [21] Copyright 2014, Royal Society of Chemistry. **f** Reprinted with permission from ref. [3] Copyright 1999, American Institute of Physics

optical transmission. In addition, 1D nanowires based on π-conjugated organic molecular aggregates can act as the high-performance optical waveguides (Fig. 3f) [3]. Further investigation on 1D organic crystal reveals that electrons and holes can be easier to form Frenkel exciton (Fig. 3c) [50–52]. When the cavity provides the exciton with adequate energy, photons and excitons in the cavity can strongly couple to form the exciton polaritons (EPs) [53]. Compared with uncoupled light, the refractive index of 1D organic crystal has enhanced by coupling light [29, 51, 54, 55], showing remarkable propagation properties [56]. This can help to break the diffraction limit so that 1D organic micro/nanostructure with subwavelength diameters is conducive to the further building blocks for miniaturized optoelectronic devices. However, because the high substrate effect caused the higher optical loss, many efforts have tried to overcome this drawback. For example, Huang et al. [57] and our group [42] fabricated hollow vertical organic nanoarrays and hollow microtubes whose optical waveguide performance have improved.

The waveguide capability of micro/nanostructure can be expressed by the loss coefficient (R). As shown in Fig. 3d [21] and Fig. 3e [49], the PL intensity at the excitation and emission points of the sample was measured. The loss coefficient (R) was calculated by single-exponential fitting $I_{tip}/I_{body} = A \exp.(-RX)$, where X is the distance between the excited site and the emitting tip. And the lower value of R indicates the better propagation. However, scale effect should not be neglected

in waveguide losses. For example, Song et al. [49] fabricated 2-((5-(6-iodo-2-oxo-2H-chromen-3-yl) thiazol-2-yl) amino)-Benzoate (ICTAB) microfiber to prove the size-dependent effect of the waveguide (Fig. 3g), which indicates that the value R increased rapidly with decreasing the cross-sectional size of the microfibers.

In this section, we briefly described the fundamental mechanism of optical waveguide, which will be helpful to understand 1D waveguide behaviors and the optical properties to be discussed in the following section.

1D waveguide behaviors and optical properties based on organic crystals

Scientific researchers have contributed to the rise of 1D organic micro/nanostructure materials in the past decade, prompting the potential applications of the materials as building blocks for miniaturized optoelectronic devices, such as logic gates [58], chemical sensors [59], photodetectors [60], organic solid-state lasers (OSSLs) [61–63], organic field-effect transistors (OFETs) [64], organic light-emitting transistors (OLETs) [65, 66] and optical waveguides [67]. Especially, optical waveguide based on 1D organic crystals has attracted enormous attention in the last few years due to their unique waveguide behaviors and optical properties. In the organic crystals, molecule staking mode, molecule structure, and molecule interaction can contribute substantially to the charge-transporting mobility. Unlike inorganic crystals, 1D organic crystals are aggregated by weak intermolecular forces [20], such as hydrogen bonds, halogen bonds, π-π interactions, and van der Waals interactions [68]. In this regard, we will introduce 1D crystals with solid-state, solid electrically controlled, flexible, hollow, uniformly doped, core-shell, multiblock and branch structures. Their waveguide behaviors and optical properties are also discussed.

1D solid-state optical waveguides

In the past decades, researchers are devoted to studying the 1D inorganic solid micro/nanoscale waveguides [69, 70], and the preparation method of the 1D structure is relatively mature. In comparison with 1D inorganic solid waveguide at micro/nanoscale, 1D organic materials possess many advantages, such as tailor-made structure [62, 71] and intense fluorescence [72, 73]. For example, Bao et al. [33] fabricated high-quality microwires of perylene diimide (PDI) molecules (Fig. 4a) through template-assisted self-assembly method on the surface of graphene oxide. The nanowire crystals are a high-quality medium for optical waveguides. And when the laser excites the different positions of the 1D microwire from the left to the right (Fig. 4b), the corresponding PL signals can be detected from the right terminus of the microwire (Fig. 4c), indicating that the intensity of the PL signals at the right tip of the microwire increases with the gradual decrease of the propagation distance. Li et al. [34] obtained rhodamine B (RhB) doped Diphenylalanine (FF) microrods with smooth surfaces (Fig. 4d). When the laser excites the different positions of the 1D microrod from the left to the right, the out-coupled intensity of the right tip of the microrod is gradually enhanced compared to the out-coupled intensity of the left tip of the microrod (Fig. 4e, and f). In terms of the microtubes with regular morphology and bright spot at microrod tips, suggesting that the microrod have good optical waveguide performance. According to the previous work, our group [36] designed and synthesized 1,4-bis((*E*)-4-(1,2,2-

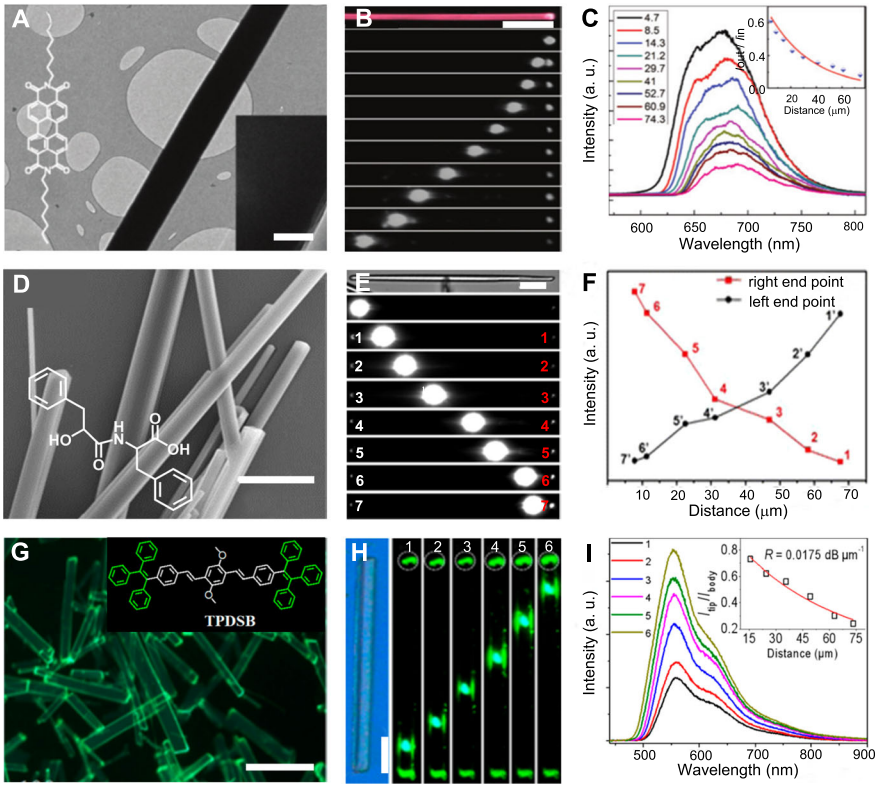

Fig. 4 1D solid-state microstructures for optical waveguides. **a** Bright-field Transmission Electron Microscope (TEM) image of a PDI wire with a scale bar of 2 μm. **b** Dark field and PL images of a PDI wire with a scale bar of 2 μm. **c** Spatially resolved PL spectra from the tip of the microwire for different separation distances between the excitation spot and tip of the wire. Inset shows I_{out}/I_{in} versus propagation distance and exponential fit (red line). **d** Bright-field SEM image of a single FF-RhB microrod with a scale bar of 10 μm. **e** Bright-field and PL images of a single FF-RhB microrod with a scale bar of 10 μm. **f** The excitation distance-dependent PL intensity at each end point. The distance denotes the length between the right end point and the excitation spot. **g** FM image of the TPSDB organic micro-ribbons with a scale bar of 100 μm. **h** PL images by exciting the identical TPDSB micro-ribbon at different points with a 375 nm laser. The scale bar is 20 μm. **i** Spatially resolved PL spectra from the tip of the micro-ribbon for different separation distances between the exciting point and the right tip of the micro-ribbon shown in **h**. Inset shows I_{out}/I_{in} versus propagation distance and exponential fit. **a, b, c** Reprinted with permission from ref. [33] Copyright 2010, Wiley-VCH. **d, e, f** Reprinted with permission from ref. [34] Copyright 2015, American Chemical Society. **g, h, i** Reprinted with permission from ref. [36] Copyright 2019, American Chemical Society

triphenylvinyl)styryl)-2,5-dimethoxybenzene (TPDSB) with aggregation-induced emission (AIE) phenomenon (Fig. 4g). Through the solution-processing approach, these AIE molecules form the 1D green-emissive solid-state microstructures (Fig. 4h), which possess superior optical properties (Fig. 4i). In addition to the simple transmission of optical waveguide in 1D solid crystals, we can achieve the chiral waveguides. Prof. Chandrasekar et al. reported a chiral waveguide based on chiral structure, which shows circular dichroism effects in the nonlinear optical emission [74]. The chiral structure with the smaller optical waveguide loss suggests the better optical waveguide performance. Therefore, the chiral waveguide based on chiral structure contributes to the development of nonlinear optical nanophotonic devices with chirality information encoded.

1D electrically controlled optical waveguides

Electrically controlled optical waveguides have become critically important for optical communication, information processing, and high-density connection of optoelectronic devices [28, 35, 75–77]. However, it is a great challenge to efficiently achieve electrically controllable light propagation for practical applications in high-density photonic devices because of the non-interactive nature of photons. Herein, we give examples to demonstrate novel and effective strategies for 1D micro/nanostructures to manipulate photon transport. Hu et al. [28] controllably synthesized the single-crystalline 2,8-dichloro-5,11-dihexyl-indolo (3,2-b) carbazole (CHICZ) microribbons (Fig. 5b) for high performance optoelectronic device. It is shown in Fig. 5a that an individual CHICZ crystal ribbon with gold stripes as source and drain electrodes has two modes for optical waveguide directions, which are along the conducting channel (mode I) and perpendicular to the conducting channel (mode II), respectively. In terms of mode I

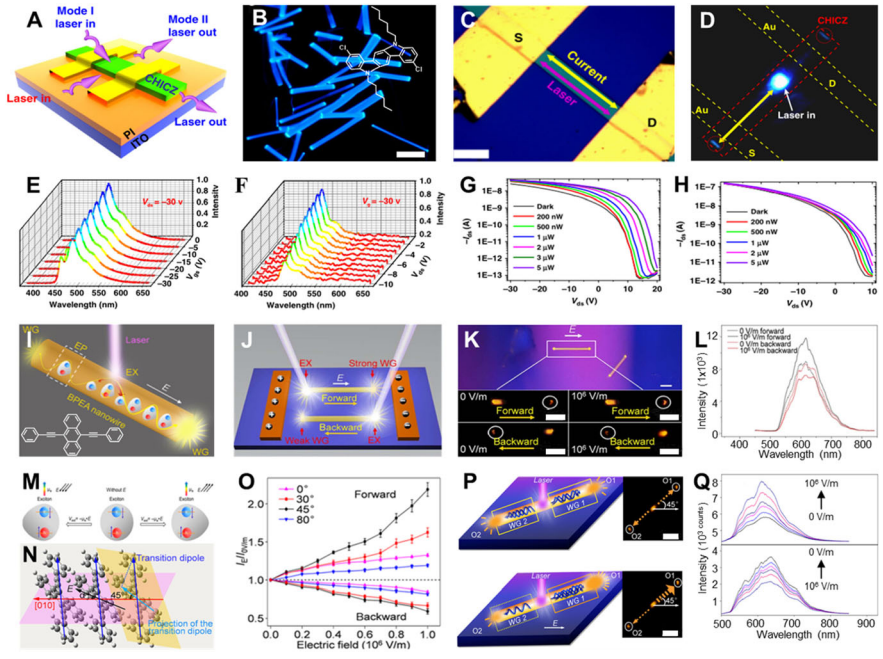

Fig. 5 1D solid-state microstructures for electrically controllable optical waveguides. **a** Schematic of an organic field-effect optical waveguide (OFEW). **b** FM image of the CHICZ crystal ribbons with a scale bar of 50 μm. **c** Current transport is parallel with the optical waveguide direction in mode I. Scale bar: 20 μm. **d** Laser in and laser out of the devices working in mode I. **e-f** Working in mode I. Optical waveguide modulation on field-effect performance, the plot of PL intensity dependence on gate voltage **e**, the plot of PL intensity dependence on source–drain voltage **f**. **g-h** Transfer characteristic dependence on a different laser illumination working in mode I **g**, and mode II **h**, respectively. **i** Schematic depiction of the asymmetric optical waveguide in BPEA nanowires under an electric field. **j** The optical waveguide asymmetric power propagation under the electric field. **k** The white circles mark the optical waveguide intensity from the microwire end tip without and with forward and backward electric fields (1.0×10^6 V/m), respectively. Scale bar: 10 μm. **l** Corresponding outcoupled PL spectra collected from the end tips of the microwire. **m** Schematic of the exciton diffusion in the absence and presence of an external electric field. **n** Schematic depiction of the spatial relationship between BPEA molecular transition dipole moment (blue arrows) and the growth direction (red arrow) of the microwire. **o** Plot of forward and backward PL intensity modulations at 610 nm versus θ, and exponential fit. **p** Dual-outcoupled intensity in the absence and presence of an electric field. Scale bar: 10 μm. **q** Output PL spectra of O1 and O2 under different field strengths ranging from 0 to 1.0×10^6 V/m. **a-h** Reprinted with permission from ref. [28] Copyright 2018, Nature Publishing Group. **i-q** Reprinted with permission from ref. [35] Copyright 2018, American Association for the Advancement of Science

(Fig. 5c-d), the direction of the current transport is perpendicular to that of the laser. Under different source–drain voltage (V_{ds}), PL intensity gradually becomes smaller when V_{ds} ranges from 0 to − 30 V with a constant V_g (gate voltage) = − 30 V, and its magnitude of the decrease can be explained by the modulation-degree M ($M = (1- (I_{on}/I_{off}) \times 100\%$), under which case M is over 25% (Fig. 5e). The M value is over 75% when V_g is shifting from 0 to − 30 V with a constant V_{ds} = − 30 V (Fig. 5f). This indicates the modulation of field effect optical waveguide. At the same time, under different laser intensities, with V_{ds} scanning from 20 to − 30 V and V_g = − 30 V in mode I (Fig. 5g), the current modulation ratio R ($R = ((I_{laser} - I_{dark})/I_{dark})$ is significantly increased up to 14, 800 under 5 μw laser illumination. However, when other conditions remain unchanged, the current modulation ratio R is only increased up to 100 under 5 μw in mode II (Fig. 5h), suggesting an effective modulation on the performance of the optical waveguide transistor.

Additionally, Zhao et al. [35] realized the controllable self-assembly of the 9,10-bis (phenylethynyl) anthracene microwires with asymmetric photon transport. It is well known that the weak interaction between photons is little affected by the external electric field because photons are chargeless and massless gauge bosons. But photons can be coupled with excitons to form a new type of hybrid state known as EPs. The formation of EPs is shown in Fig. 5i, where the external electric field can control the exciton diffusion, leading to the directional flow of photons and forming the asymmetric optical waveguide. As shown in Fig. 5m, the exciton diffusion can be changed by the interaction potential V_{ext} ($V_{ext} = - \mu_e \cdot E$, where μ_e is the transition moment of the exciton and E is the external field.). V_{ext} can be modulated by two factors which are the electric field strength and the electric field direction. This process is shown in Fig. 5j-l, when the electrical field with certain direction is exerted, the waveguide output along the electrical field will be enhanced, whereas the waveguide output reverse to the electrical field will be weakened. According to the previous work on polarized emission of organic single crystal [33, 78–81], the PL intensity has the maximum value when the direction of incident light is parallel to the transition dipole moment of the organic crystal. The calculated result shows that the polarized angle θ between the transition dipole moment of the nanowire and the axis of the nanowire is 45°. By making the electric field and light propagation direction co-planar (Fig. 5n) and adjusting the direction and strength of the electric field, higher propagation can be achieved when the EPs propagate along the field direction (Fig. 5o). Moreover, when the laser excites the middle of the nanowire, waveguide intensities at wire tips are obviously different with electric filed compared to waveguide intensity of wire tips without electric filed, which is the asymmetric waveguide (Fig. 5p). The variable asymmetric out-coupled spectra and the modulation ratios spectra ($(I_E - I_0)/I_0$) of two wire tips are also obtained by changing the input electrical filed (Fig. 5q). All the above results successfully demonstrate the electrically controlled optical waveguides in 1D solid-state.

1D flexible optical waveguides

Organic crystals with characteristics of brittle and crack are difficult to create flexible waveguides under the external stimuli, which makes it high requirement for the nature of material. Thus, the investigation of elastic organic crystals is one of the currently

developing trends in flexible photonics. Elastic organic crystals under the external stimuli usually have various outstanding mechanical behaviors, e.g., bending [37, 38, 82–85] and twisting [86, 87]. As a pioneer work, Prof. Zhang et al. firstly demonstrated the flexible microrods of (*E*)-1-(4-(dimethylamino)phenyl)iminomethyl-2-hydroxyl-naphthalene (DPIN) crystals (Fig. 6a_1-a_6), which is owing to their planar molecular conformation and periodic monoclinic packing pattern [38]. Moreover, the stretching of outer layer molecular distance and the compression of internal molecular distance by applied external force in the DPIN organic crystal are shown in Fig. 6b. The stretching of

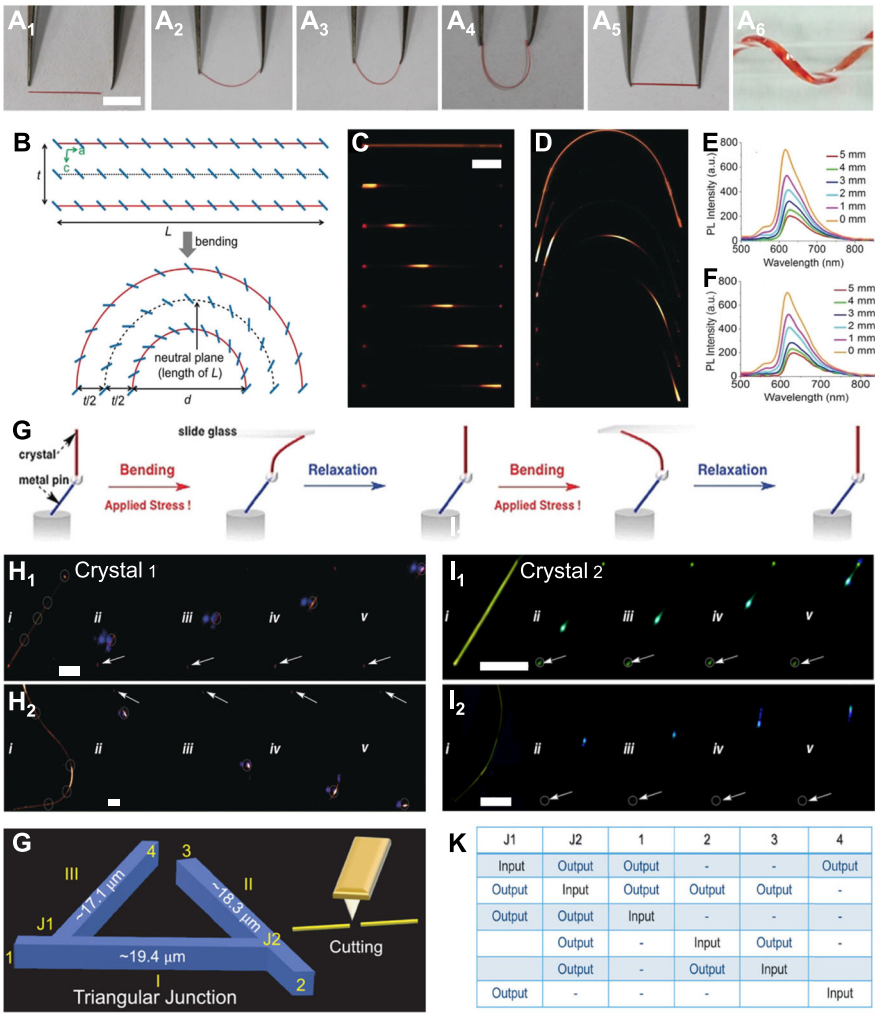

J1	J2	1	2	3	4
Input	Output	Output	-	-	Output
Output	Input	Output	Output	Output	-
Output	Output	Input	-	-	-
	Output	-	Input	Output	-
	Output	-	Output	Input	
Output	-	-	-		Input

Fig. 6 1D solid-state microstructures for flexible optical waveguides. **a_1-a_6** Illustration of the mechanical test of the crystal. **b** Graphical representation of bending process of elastic crystal. Optical waveguide properties of the identical crystallin straight shape **c** and in bent shape **d**. The scale bar is 1 mm. **e-f** PL spectra recorded upon excitation of the straight shape **f** and bent shape **g** at different positions. **g** Illustration of the crystal fixed on a metal pin and mechanical test. **h_1** Straight crystal 1: PL images obtained by exciting an identical microrod at different positions. Scale bar: 1 mm. **h_2** Bent crystal 1 with 1.9% strain: PL images obtained by exciting an identical microrod at different positions. Scale bar: 1 mm. **i_1** Straight crystal: PL images obtained by exciting an identical microrod at different positions. Scale bar: 1 mm. **i_2** Bent crystal with 1.5% strain: PL images obtained by exciting an identical microrod at different positions. Scale bar: 1 mm. **g** Schematic illustration of cutting and bending/straightening of microrod. K Table depicts various input and output positions. **a_1-e** Reprinted with permission from ref. [38] Copyright 2018, Wiley-VCH. **d_1-i** Reprinted with permission from ref. [37] Copyright 2018, Wiley-VCH. **g-k** Reprinted with permission from ref. [39] Copyright 2020, Wiley-VCH

molecular out-layer structure and the compression of the internal-molecular structure can be realized by the π … π interactions between molecules. In addition, the C-H … O hydrogen bonds and the close packing features also are key factors for the achievement of elastic DPIN crystal. And the optical waveguides of the straight crystal and bent crystal were displayed in Fig. 6c and d. The optical loss values of the straight crystal (0.270 dB/mm) and bent crystal (0.274 dB/mm) have the close value (Fig. 6e-f), suggesting the highly elastic property and waveguide performance of DPIN organic crystal.

Additionally, Hayashi et al. [37] designed and synthesized a structure of tetrafluoropyridyl derivative 1 and pentafluorophenyl derivative 2 with π-conjugated structure and they made great efforts to prepare crystal 1 (orange emission) and crystal 2 (green emission) through the vapor diffusion process. Moreover, they calculated the interatomic distance and the intermolecular torsion angle of crystal 1 and crystal 2, indicating that the molecular structures in both crystal 1 and crystal 2 have a highly planar and rigid conformation. Consequently, crystal 1 and crystal 2 under repeatedly bending-relaxation test show good elasticity (Fig. 6a), and testing bent and straight optical waveguides of both crystal 1 and crystal 2 by exciting different positions of crystal 1 and crystal 2 with a laser beam (Fig. 6b_1, b_2, c_1, and c_2). It suggests that the flexible optical waveguide performance of crystal 1 (R_{Bent} = 0.047 dB/mm and $R_{Straight}$ = 0.043 dB/mm, with no bending mechanofluorochromism) is better than that of crystal 2 (R_{Bent} = 1.003 dB/mm and $R_{Straight}$ = 0.703 dB/mm, with bending mechanofluorochromism) owing to the lower molecular planarity of crystal 2.

The precise microscale operation technique of flexible crystal contributes to realize the flexible photonic devices. At present, Prof. Chandrasekar et al. fabricated 1,4-bis (2-cyanophenylethynyl) benzene elastic crystal through the vapor diffusion process [39]. In the waveguide's experiment, the 1,4-bis (2-cyanophenylethynyl) benzene elastic crystal with blue emission possesses lower optical waveguide loss, indicating that the microrods have the better optical waveguide performance. Using atomic force microscopy manipulation technique, the geometrical shape of elastic crystal can be tuned from bent crystal to straight crystal, and the length of crystal can be modified via the precise cutting of atomic force microscopy cantilever. As is shown in Fig. 6g, the geometrical shape of elastic crystals can become triangle geometries through the precise cutting of atomic force microscopy cantilever. The lengths of elastic crystals with triangle geometries are 19.4 μm, 18.3 μm and 17.1 μm, respectively. The elastic crystals with triangle geometries have two junctions (J1 and J2) and four output/input tips (1, 2, 3 and 4), respectively. When the input signal is respectively injected into J1, J2, 1, 2, 3 and 4, respectively, the elastic crystals with triangle geometries are selectively output emission. The Fig. 6k summarizes the various output and input optical signals, which can be used in the optical logic gate operation.

1D hollow optical waveguides

In comparison with 1D solid structures1, D hollow tubular structures display the outstanding waveguide behaviors owing to reduced optical loss in the otherwise solid center and improved optical propagation inside the remaining outer shell [23–25, 40, 41, 88–90]. As shown in Fig. 7a, researchers [40] prepared a hollow tubular microrod

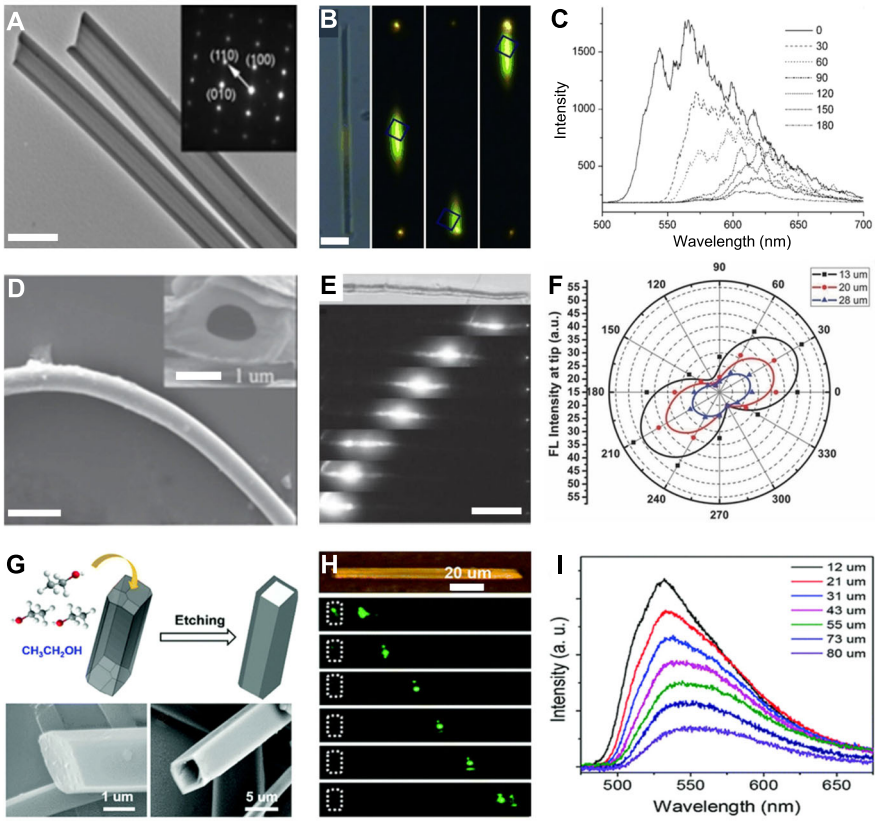

Fig. 7 1D hollow microstructures for optical waveguides. **a** Bright-field TEM image of the BPEA microtube, scale bar: 2 nm. **b** Bright-field image of BPEA microtube, and micro-area PL images of BPEA microtube obtained by exciting identical tubes at three different positions, scale bar: 10 μm. **c** Spatially resolved PL spectra of out-coupled light by excitation at the distance of 0–180 mm from the end of the tube. **d** Bright-field SEM image of the PDA microtube, scale bar: 10 μm. **e** Bright-field image of the DPEpe–F_4DIB microtube, and FL microscopy image of the DPEpe–F_4DIB microtube collected upon excitation of identical microtube at seven different positions, scale bar: 10 μm. **f** Plot of PL intensity versus the polarizer rotation angle excited at three different positions. **g** Formation mechanism of the DPEpe–F_4DIB microtubes, and bright-field SEM image of the microrod (scale bar: 1 μm) and microtube (scale bar: 5 μm). **h** Bright-field image (top) and PL images of the DPEpe–F_4DIB microtube excited, scale bar: 20 μm. **i** Spatially resolved PL spectra from the left-tip of the microtube with different separation distances in **h**. **a-c** Reprinted with permission from ref. [40] Copyright 2008, Wiley-VCH. **d-f** Reprinted with permission from ref. [78] Copyright 2014, Wiley-VCH. **g-i** Reprinted with permission from ref. [42] Copyright 2018, The Royal Society of Chemistry

crystal based on the small organic molecule of 9,10-bis (phenylethynyl) anthracene, which possess glossy surface. And the tips of BPEA microtube have bright luminescence spots by exciting the different positions of this microtube via a laser beam (Fig. 7b) and the corresponding distance dependent PL spectra are shown in Fig. 7c, signifying the better waveguide performance. Moreover, Ming et al. [41] put great efforts to prepare 1D Polydiacetylene (PDA) microtubes via the hierarchical self-assembly method. Microtubes with homogenously smooth surface are shown in the scanning electron microscopy (SEM) image (Fig. 7d). It is indicated that the microtubes display the bright emission at tips (Fig. 7e-f) when the microtubes at center are excited by a laser beam. Furthermore, according to these pioneering works, our group [42] fabricated microrods and microtubes by the solution-processing approach. The 1D organic cocrystal DPEpe–F_4DIB microrods can be changed into microtubes after ethanol

etching, because the surface energy at the center of the microrods is relatively high compared to that of the outer surfaces. As shown in Fig. 7g, the microtubes have regular morphology with smooth surface, leading to the good optical waveguide performance with a low loss coefficient of 0.0145 dB/μm (Fig. 7h, and i).

1D uniformly doped optical waveguides

There have been many reports about 1D organic uniformly doped microstructures [10, 29, 43, 91, 92]. Their applications are mainly in optical modulation and full-color display for integrated optoelectronic devices. Herein, Yao et al. [43] fabricated 1D binary microtubes and microrods, respectively. The molecular structures of perylene and 2,4,5-triphenylimidazole (TPI) are shown in Fig. 8a. The perylene molecules, serving as an assistant, are evenly dispersed in the TPI matrix to etch the solid rod into microtube with the doping ratio of 1.25% in the host-guest system. Moreover, the etched hollow center of the microtubes leads to lower waveguide loss relative to microrods, resulting in a much longer propagation length (Fig. 8c-f). The schematic of both intermolecular fluorescence resonance energy transfer (IFRET) and remote energy relay (RER) process

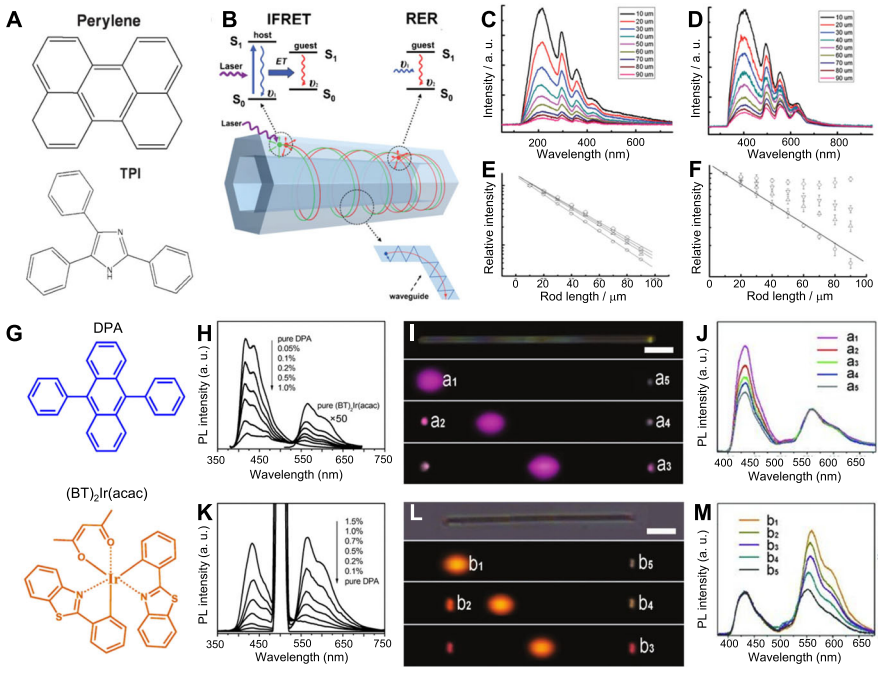

Fig. 8 1D uniformly doped microstructures for optical waveguides. **a** Molecular structure of perylene and TPI. **b** Schematic representation of the annular cavity of the binary microtube, and energy diagrams for the IFRET and RER processes. **c-d** Spatially resolved PL spectra of out-coupled light for a single binary microrod and microtube, respectively. **e-f** The corresponding linear fit of the PL spectra of microrod and microtube versus excitation position, respectively. **g** Molecular structures of DPA and $(BT)_2Ir(acac)$. **h** Emission spectra of the DPA nanowires with different doping contents $(BT)_2Ir(acac)$ excited with a 360 nm laser. **i** Bright-field and PL images of the microwire with $(BT)_2Ir(acac)$ contents of 0.2%, Scale bars: 5 μm. **j** Corresponding spatially resolved PL spectra collected from tips of microrod in **i**. **k** Emission spectra of the DPA nanowires with different doping contents $(BT)_2Ir(acac)$ excited with a 500 nm laser. **l** Bright-field and PL images of the microwire with $(BT)_2Ir(acac)$ contents of 1%, Scale bars: 5 μm. **m** Corresponding spatially resolved PL spectra collected from tips of microtube in **l**. **a-f** Reprinted with permission from ref. [43] Copyright 2009, Wiley-VCH. **g-m** Reprinted with permission from ref. [29] Copyright 2011, Wiley-VCH

is shown in Fig. 8b. 1D microstructure excited by a laser beam can conduct not only the UV emission but also the green emission because of the energy transfer between TPI and perylene components. The remote energy relay process refers to waveguide modulate in the binary microtube, suggesting that the doped perylene constituent in the binary microtube will reabsorb the ultraviolet photon of the TPI component and subsequently re-emit the photons in the green-emissive bands. Yao et al. [29] also reported the wavelength modulation in the Iridium (III) bis (2-phenyl benzothiozolato-N, $C^{2'}$)acetylacetonate($(BT)_2Ir(acac)$) doped 9,10-di-phenylanthracene (DPA) organic nanowire via the fluctuations of singlet and triplet excitons during propagation (Fig. 8g). Using different doping ratio, the spectra of the doped nanowires upon a 350 nm laser excitation indicate that the orange emission is significantly enhanced (Fig. 8h), suggesting efficient singlet exciton energy transfer from DPA molecules to $(BT)_2Ir(acac)$ molecules. Furthermore, the optical signal of the spectra of the doped nanowires upon a 500 nm laser excitation demonstrates the blue emission, showing efficient triplet exciton energy back transfer from $(BT)_2Ir(acac)$ molecules to DPA molecules (Fig. 8k). The micro-area PL images obtained from two identical $(BT)_2Ir(acac)$ doped nanowires with the doping concentration of 0.2% and 1.0% (Fig. 8i, l) display the blue emission and the orange emission respectively because of the exciton fluctuations, and their corresponding PL spectra are shown in Fig. 8j and m. In summary, this novel type of organic waveguide, acting as an optical regulator, is helpful for developing novel multi-component waveguide working as building blocks in integrated nanoscale devices [93].

1D core-shell optical waveguides

The core/shell micro/nanostructures can be divided into zero-dimension (0D) particles [94–96], 1D wires [31, 97], and two dimensional (2D) plates [98, 99] from the dimensionality. Great progress in the organic core/shell structures has been made after two decades' development in both fundamental research and applications. 1D organic core-shell heterostructures are superior in physicochemical features, such as evanescent coupling and carrier transport [31], and energy transfer [44]. There have been numerous reports about optical waveguides based on 1D organic core-shell heterostructures and their potential applications are mainly in chemical gas sensor [19, 31], multi-color optical waveguide [44] and optical logic gate [32, 100]. Figure 9a shows an example of the organic core/shell nanowires with waveguiding core and chemiluminogenic cladding that can be applied to the chemical gas sensor [31]. The organic core/shell nanowires consisting of the single-crystalline 9,10-bis (phenylethynyl) anthracene (BPEA) and bis (2,4,5-trichloro-6-carbopen-toxy-phenyl) oxalate (CPPO) molecules have great mechanical and optical properties. However, CPPO crystal itself is poor in mechanical and optical properties. This is because that the evanescent coupling between the core and shell resulted from the introduction of BPEA molecules is a key factor to improve optical property. The optical waveguide response of the nanowires exposed to H_2O_2 vapors is remarkably fast (35 ms) due to the high sensitivity and selectivity of CPPO molecules to H_2O_2 vapors. Therefore, to prove the chemiluminescence sensitivity and intensity of a single core/shell nanowire to H_2O_2 vapors, the incident light is inputted from one end of the core-shell nanowires and the output emission is measured at the other end in a sealed glass chamber with a 6 ppm H_2O_2 gas flowing system. The

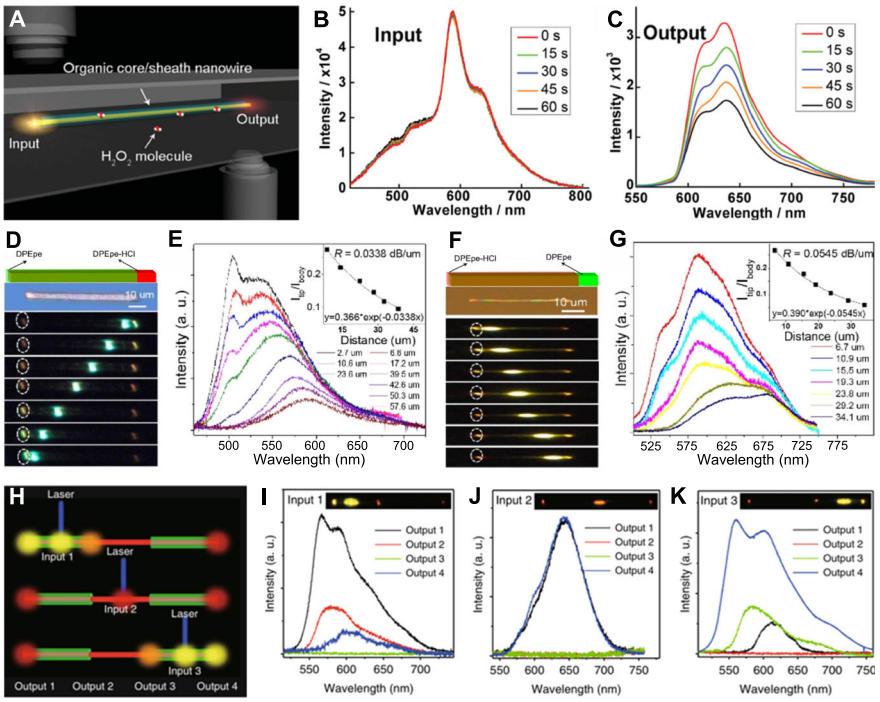

Fig. 9 1D core/shell microstructures for optical waveguides. **a** Schematic of the waveguide sensor. **b-c** Time-dependent PL spectrum of the input light **b** and output light **c** on exposure to 6 ppm H_2O_2 vapor. **d, f** Bright-field and PL images obtained from both **d** DPEpe-HCl/DPEpe core/shell and **f** DPEpe/DPEpe-HCl core/shell microcrystal with different colors emission by exciting the wires at seven different positions. Scale bar: 10 μm. **e, g** Corresponding spatially resolved PL spectra in **d** and **f** with different separation distances. Insets: The ratios of the intensity I_{tip}/I_{body} against the distance. **h** Schematic diagram of optical logic gate based on the organic core-shell microwire. **i-k** Spatially resolved PL spectra of the four output channels obtained by exciting microwire at three different laser beam input positions: at the left end; at the center; at the right end. Insets: the corresponding FM images. **a-c** Reprinted with permission from ref. [31] Copyright 2012, Wiley-VCH. **d-g** Reprinted with permission from ref. [44] Copyright 2019, American Chemical Society. **h-k** Reprinted with permission from ref. [32] Copyright 2019, Nature Publishing Group

corresponding PL spectra of the input and output light at different time are shown in Fig. 9b and c, suggesting that the core-shell nanowires with rapid and high selectivity of optical sensor of a trace of H_2O_2 gas.

Furthermore, our group [44] reported a 1D core-shell micro/nanostructures based on the π-conjugated organic molecules of DPEpe and DPEpe-HCl. The formation of DPEpe crystal and DPEpe-HCl crystal is reversible protonation/deprotonation process. As shown in Fig. 9d and f, self-assembled green-emissive single-crystal DPEpe microrods and red-emissive single-crystal DPEpe-HCl microrods can both act as the core or the shell. And the PL spectra of DPEpe/DPEpe-HCl core-shell microrods (Fig. 9g) has a significant red shift compared to those of DPEpe-HCl/DPEpe core-shell microrods (Fig. 9e), which implies the remarkable optical tunability of the core-shell system.

Recently, our group [32] also reported the horizontal epitaxial growth process via the hierarchical self-assembly of 1D core-shell micro/nanostructures. The DPEpe-F_4DIB cocrystal based on the hydrogen bond between DPEpe molecule and F_4DIB molecule displays the green emission and the DPEpe-BrFTA cocrystal based on the halogen bonds between DPEpe molecule and BrFTA molecule shows the red emission. 1D DPEpe-BrFTA/DPEpe-F_4DIB core-shell nanowires with a low lattice mismatching rate

between the two cocrystal are controllably synthesized by the precise manipulation of noncovalent interactions: hydrogen bonds, halogen bonds and π–π interaction. The multicolor emission properties of the heterostructure nanowire at Input 1, Input 2 and Input 3 excitation positions are shown in the plot of Fig. 9h and the output spectra of Output 1, Output 2, Output 3 and Output 4 channels were collected (Fig. 9i-k). When Input 1 and Input 3 positions of the core-shell nanowire were excited by a laser beam, the photon propagation process from excitation position to the two ends corresponds to the active and passive modes, respectively (Fig. 9i, and k). When excited at Input 2 of the core-shell nanowire, the photon propagation to the two ends is passive (Fig. 9j). This feature of 1D core-shell heterostructure waveguides can be applied in the optical logic gate operation at microscale.

1D multiblock optical waveguides

The optical waveguide of 1D multiblock micro/nanostructures consisting of the binary components make them serve as excellent candidates for optical applications [45, 46, 101–104]. Here, we previously reported 1D in-series organic multiblock heterostructures based on the *trans-o*-BCB and *cis-o*-BCB (Fig. 10a), whose construction employs a highly controllable photochromic method [45]. As shown in Fig. 10b and c, the 3-block heterostructure and the 5-block heterostructure can be realized by selectively covering the sections of the microrods, resulting in the molecular structure transformation from *trans-o*-BCB to the *cis-o*-BCB. The FL microscope images of *cis-o*-BCB structures and *trans-o*-BCB microcrystals exhibits the blue and green emission, respectively. The optical signal of the Out 1, where radiative energy transfer occurred, is blue/green-emissive, which indicates the passive/active mixed waveguide mode resulted from the energy transfer between *cis-o*-BCB structure and *trans*-o-BCB structure (Fig. 10b). When the input signal is injected in the In 1, In 2 and In 3, separately, The optical signal of the all output channels are blue-emissive, which denotes the passive waveguide mode (Fig. 10c). The efficient energy transfer in the 1D multiblock micro/nanostructures is a universal mechanism, it can realize the selective output wavelength and the multi-color emission. Furthermore, Yao et al. [46] reported the multi-color phosphorescence of 1D multiblock microstructures (Fig. 10d) with the emission from green to red based on efficient triplet energy transfer between the donor ($[Ir(ppy)_2(pzpy)]^+$) and acceptor ($[Ru(bpy)_3]^{2+}$). Figure 10e displays the energy diagram of the Ir donor and Ru acceptor. The triplet state energy (T_1) of Ir donor (2.61 eV) is higher than the S_1 (2.53 eV) and T_1 (2.1 eV) level of Ru acceptor. It is suggested that the energy of Ir donor can transfer to the Ru acceptor. The FL microscopy image of a heterojunction nanorod illustrates the multi-color phosphorescence (Fig. 10f). When the input laser is injected into In 1, In 2 and In 3, the corresponding output ports Out 1, Out 2 and Out 3 show green, red and green/red mixed emission, respectively.

Additionally, Prof. Chandrasekar et al. reported a photoresponsive microrod based on dithienylethene molecule unit [22]. As shown in the Fig. 10g, the closed-state (L-c) and the open-state (L-o) microrods can be formed by their molecules. Moreover, the formation of closed-state (L-c) and open-state (L-o) microrods is reversible process under exposure to UV (355 nm) and visible light (448 nm). The open-state (L-o) microrod was excited by a laser beam (448 nm), which exhibits a

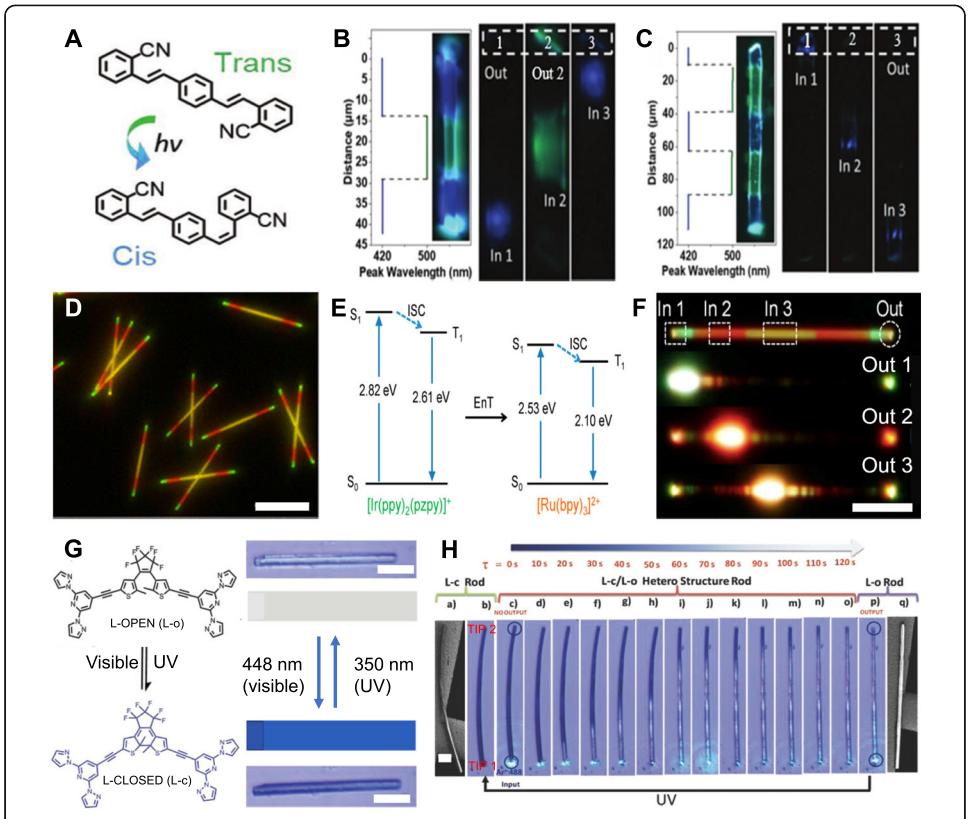

Fig. 10 1D multiblock microstructures for optical waveguides. **a** Molecule structures of *trans-o*-BCB and *cis-o*-BCB. **b-c** PL peak wavelength change along the three-block heterostructure and the five-block heterostructure; FM images of the three-block and the five-block heterostructures excited at three different positions. **d** FM images of the microrod with a scale bar of 10 μm. **e** Energy diagram of the Ir donor and Ru acceptor, ISC: intersystem crossing. ET: energy transfer. **f** FM images of the microrod at three different positions with a 405 nm laser. The scale bar is 10 μm. **g** Molecular structure of open-state (L-o) and closed-state (L-c), and bright-field image of open-state and closed-state microrods. The scale bars are 10 μm. **h** SEM images of open-state and closed-state microrods and bright-field image of open-state and closed-state microrods at different photoradiation time. **a-c** Reprinted with permission from ref. [45] Copyright 2019, Wiley-VCH. **d-f** Reprinted with permission from ref. [46] Copyright 2018, American Chemical Society. **g-h** Reprinted with permission from ref. [22] Copyright 2015, Wiley-VCH

passive waveguide. However, the closed-state (L-c) microrod can absorb the energy of a laser beam (448 nm), converting to the open-state (L-o) microrod by a time-dependent solid state cyclo-reversion reaction, which can realize the output of transmission light at the end part. According to this photoresponsive feature, 1D multiblock heterostructure is composed of the closed-state (L-c) and the open-state (L-o) structure. The formation of 1D multiblock heterostructure is illustrated in Fig. 10h. the Tip 1 at the closed-state (L-c) microrod was excited by a 448 nm laser beam. At≈0 s, input laser signal cannot propagate optical signal to Tip 2 of the closed-state (L-c) microrod. When the photoradiation time changes from 0 to 120 s, the length of open-state (L-o) microrod in 1D multiblock heterostructure gradually increases from 0 to 153 μm. Finally, At≈120 s, the closed-state (L-c) microrod completely converts to the open-state (L-o) microrod, suggesting that input laser signal at the Tip 1 of open-state (L-o) microrod can transmission optical signal to Tip 2. Therefore, the photoresponsive 1D organic heterostructures with high controllability have the potential application for waveguide modulator.

1D branched optical waveguides

1D branched heterostructures and homostructures at micro/nanoscale can be prepared by various methods, including solvent slow evaporation method [48, 105, 106], two-step solution and vapor deposition process [30] and one-pot solution method [47]. 1D branched micro/nanostructure with fine photonic properties can be used in optical routers [30, 47, 107, 108], asymmetric optical waveguide [48, 106] and multichannel signal converter [109, 110]. Dendritic organic heterojunctions with aluminum tris (8-hydroxyquinoline) (Alq_3) microwire trunks and 1,5-diaminoanthraquinone (DAAQ) nanowire branches (Fig. 11a, and b) were successfully prepared by Zhao et al. through the two-step solution and vapor deposition process [30]. Dendritic organic heterojunctions emit multicolor light with a focused laser beam excited at the trunk. This phenomenon is attributed to both waveguide propagation and energy transfer from trunk to branches in 1D dendritic heterojunctions. Moreover, as shown in Fig. 11c and d, the PL intensities at the trunk tip and branch tip periodically change as the polarization angle increases from 0 to 360 degrees, implying the potential to act as the optical routers.

Fu et al. [47] also reported a 1D organic heterojunction with COPV microribbon trunks and TPI branches synthesized via a one-pot solution method for nanoscale optical router. This formation mechanism of this heterostructure is mainly caused by the

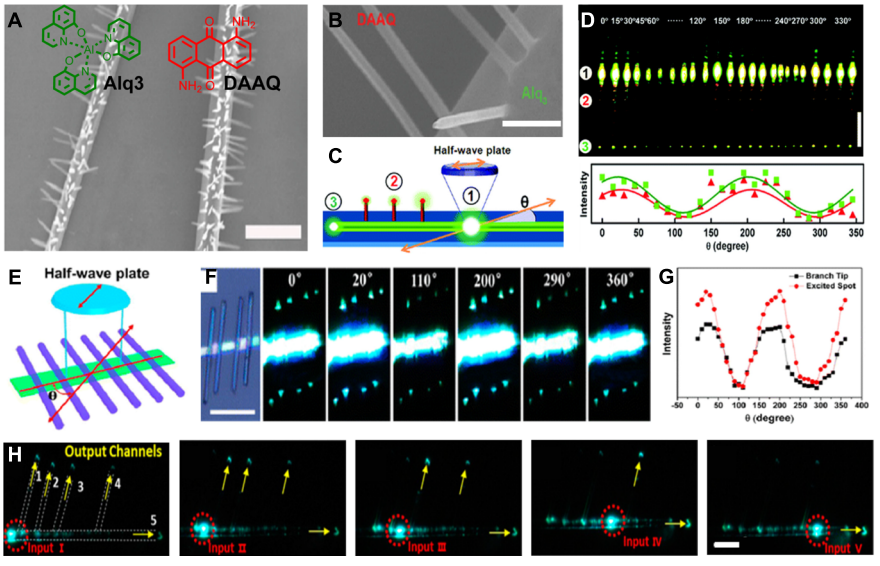

Fig. 11 1D branched microstructures for optical waveguides. **a**-**b** Molecular structures of Alq_3 and DAAQ; bright-field SEM image of the Alq_3 – DAAQ dendritic heterostructure. The scale bars: 5 μm and 1 μm, respectively. **c** Schematic illustration of the experimental setup for polarized excitation. **d** The variation of the emission intensities from Alq_3 micro-ribbon and DAAQ microwire taken by exciting the middle area 1 at different polarization angles ($\theta = 0 \sim 360°$). Scale bar: 20 μm. And polarization-angle-dependent PL intensity of the branch channel 2 and the trunk channel 3 of the Alq_3-DAAQ NWHJ-based was excited with a linearly polarized laser beam at input1. **e** Schematic illustration of the measurement setup for polarized excitation. **f** The variation of the emission intensity from COPV micro-ribbon and the tips of branches as a function of polarization angle ($\theta = 0 \sim 360°$). The scale bar is 5 μm. **g** PL intensity of the BNwHs taken by exciting the COPV ribbon at different polarization angles. **h** Microscope images of the *o*-BCB homostructure excited at different points by a 375 nm laser. The scale bar is 5 μm. **a-d** Reprinted with permission from ref. [30] Copyright 2012, American Chemical Society. **e-g** Reprinted with permission from ref. [47] Copyright 2014, American Chemical Society. **h** Reprinted with permission from ref. [48] Copyright 2018, American Chemical Society

multiple hydrogen-bonding interactions between TPI and COPV constituents. The schematic illustration of optical channeling property [47] (Fig. 11e) exhibits a measurement setup for the polarized excitation. Furthermore, the polarization-angle-dependent PL intensities of excited spot and branch tip can also be controllably changed by rotating the incident polarization ($\theta = 0 \sim 360°$) (Fig. 11f-g).

Recently, our group [48] successfully synthesized the branched nanowire homostructures consisting of the single component of *o*-BCB with asymmetric optical waveguide via a simple solvent slow evaporation method. As clearly seen in Fig. 11h, when the excitation position moves from Input I to Input V, only the output signal at the output ports that are at the right side of the input position can be detected, suggesting the asymmetric optical waveguide performance of the branched homostructure.

Advantages and disadvantages of 1D organic micro/nanostructures

1D organic solid crystals have inspired increasing interests due to their inherent features, such as weak molecular interaction, high purity and minimized defects, leading to good optical waveguide performance of 1D solid crystal. Therefore, these optical waveguides based on various structures made of 1D crystals demonstrate the low optical waveguide loss, the multi-functional optical properties, and so on. Compared with 1D solid structures, 1D hollow structures are promising for the high-performance optical waveguides on account of the reduced optical loss in the center of 1D hollow structures and the improved optical propagation inside the remaining outer shell. Therefore, 1D hollow optical waveguides are the excellent candidates for the practical applications. Generally, the 1D organic crystals with characteristics of brittle and crack, the optical waveguide based on 1D organic crystals cannot be applied in flexible photonics devices. 1D organic crystals with elastic feature are the good candidates for flexible photonics devices [27].1D crystals always have the single-color emission. Thus, this is not conducive to realize the multi-optical signal propagation of 1D crystals of one component. Doping in the organic crystals is an efficient strategy to realize the multicolor emissions, which can be applied in waveguide modulator [43]. At present, optical waveguides based on 1D organic crystals are symmetric, leading to the simple waveguide performance of 1D organic crystals. The symmetric waveguides based on organic crystals can realize the asymmetric optical transmission via the external electric field. The asymmetric waveguides of 1D organic crystals expand opportunities for creating scalable integration of photonics in a chip [28].

In comparison with 1D single structures, the multi-level structures, combined the advantages of single component materials, make up for the intrinsic deficiencies of single component materials. These fascinating organic topological heterostructures are superior in physicochemical features, which have been proved to be promising candidates as the building blocks of photonic devices. For example, the branched structures realize the photon transmission characteristics of multiple input/output channels, which is an ideal platform for optical router [47]. The multiblock structures demonstrate the modulation of active optical waveguide and passive optical waveguide, which can be applied in the optical logic gate operation at microscale [45]. The core-shell structures can improve stability of core layer and reduce its optical waveguide loss. When the shell layer of the core-shell structures is sensitive to gas molecules, the core/shell structures realize the application of chemical sensor [31].

Conclusion and outlook

As the indispensable component of optical circuits, optical waveguides have undergone tremendous development during the past decade. The most typical example is that Prof. Kao K have used optical fibers made by quartz glass for optical communication. Commercial optical fibers today, being composed of either silica or transparent polymers, have perfect data-carrying capacities. The organic optical waveguides are, relatively, a new area. Impressively, organic micro/nanostructures, especially 1D organic micro/nanostructures based on small molecules have shown unique advantages, such as tunable optical property, toiling molecule structure, high-thermal stability and controllable supramolecular self-assembly process by the solution-processing approach. These distinguishing features of 1D micro/nanoscale structures are expected to work as a promising optical waveguide in miniaturized photonic applications. Herein, we have summarized 8 different types of 1D organic micro/nanostructures developed recently for optical waveguides with specific properties, specific properties. Which have been applied for optical logic gate, optical router, multichannel signal converter, OFEW, waveguide modulator, and chemical sensor, etc. Therefore, these 1D organic micro/nanostructures can function as the outstanding optical elements in organic integrated photonics.

Notably, it highlights that the investigations of these 1D organic micro/nanostructures are in the early stage of research, which have plenty of room for further innovations. Indeed, there are still many challenges existing, which needs tremendous efforts for the exploration in this new field. Firstly, the main interaction in organic micro/nanostructure corresponds to the non-covalent interaction between molecules, such as van der Waals, hydrogen bonds, halogen bonds and π-π interactions. The 1D organic micro/nanocrystals with high-quality through a facile approach remain a huge challenge. Its nucleation growth process is very susceptible to the external environment such as solvent type, temperature, and solution concentration. The manipulation of the non-covalent interaction between molecules is an efficient strategy to fabricate the organic micro/nanocrystals. When the strong non-covalent interaction between molecules exists, the self-assembled 1D micro-nano structures can be designed and synthesized according to the molecular packing mode. It is easy to form the 1D organic structure. Although the optical waveguide based on organic materials has achieved great development, the optical performances in organic molecular crystals are still a significant drawback compared to commercial optical fibers composed of either silica or transparent polymers. This is a long way to realize practical application based on the optical waveguide of organic crystals. But in the past two decades, breakthroughs in optical waveguides based on 1D organic crystals have enabled us to have a deeper understanding of the tuning optical properties of 1D organic crystals and the construction of optical building blocks based on organic crystals. It is meaningful that these photonic components can be applied in chemical sensor, flexible single-crystal photonic circuit, organic field effect waveguide, multichannel signal converter optical logical gate, and optical waveguide modulator. Therefore, it is believed that the multi-functional organic micro/nanostructures with stability are great importance for photonic devices. In the future, scientific researchers will have efforts to design and synthesize the organic micro/nanostructure with multi-function and good stability to realize the practical photonic devices based on optical waveguides. Furthermore, the 1D organic

heterostructures comprising of multi-components remain a considerable challenge in lattice matching and surface-interface energy balance. This issue hinders the development of 1D organic heterostructures for the optical building blocks. Therefore, it is essential to develop 1D organic heterostructure with the facile fabrication methods.

In summary, photonic applications especially the optical waveguides based on 1D organic crystals have great prospect and high value. Scientists around the world have strong interests for the exploration in this field. Despite some existing challenges, we believe that developing a series of multi-functional waveguide devices will be the most disruptive progress in future.

Abbreviations

1D: One-dimensional; OFEW: Organic field-effect optical waveguide; IFRET: Intermolecular fluorescence resonance energy transfer; RER: Remote energy relay; 0D: Zero-dimension; 2D: Two dimensional; OFETs: Organic field effect transistors; OLETs: Organic light-emitting transistors; EPs: Exciton polaritons; PL: Photoluminescence; FL: Fluorescence; SEM: Scanning electron microscopy; TEM: Transmission electron microscope; UV: Ultraviolet

Acknowledgements

This project was funded by the Collaborative Innovation Center of Suzhou Nano Science and Technology (CIC-Nano), by the Priority Academic Program Development of Jiangsu Higher Education Institutions (PAPD). And by the "111" Project of The State Administration of Foreign Experts Affairs of China.

Authors' contributions

These authors contributed equally: S. Chen, M.-P. Zhuo. Methodology, L.-S. Liao; writing—original draft preparation, S. Chen, M.-P. Zhuo, X.-D. Wang; writing—review and editing, G.-Q. Wei, X.-D. Wang, L.-S. Liao; supervision, L.-S. Liao. All authors read and approved the final manuscript.

Funding

The National Natural Science Foundation of China (Nos. 21703148 and 21971185) and the Natural Science Foundation of Jiangsu Province (BK20170330).

Availability of data and materials

All data needed to evaluate the conclusions in the manuscript are presented herein and/or the Supplementary Materials. Additional data related to this study may be requested from the authors.

Competing interests

The authors declare no competing financial interests.

Received: 8 January 2021 Accepted: 7 February 2021
Published online: 06 March 2021

References

1. Zhang C, Zhao YS, Yao JN. Optical waveguides at micro/nanoscale based on functional small organic molecules. Phys Chem Chem Phys. 2011;13:9060–73.
2. Cui QH, Zhao YS, Yao JN. Photonic applications of one-dimensional organic single-crystalline nanostructures: optical waveguides and optically pumped lasers. J Mater Chem. 2012;22:4136–40.
3. Yanagi H, Morikawa T. Self-waveguided blue light emission in *p*-sexiphenyl crystals epitaxially grown by mask-shadowing vapor deposition. Appl Phys Lett. 1999;75:187–9.
4. Clark J, Lanzani G. Organic photonics for communications. Nat Photonics. 2010;4:438–46.
5. An BK, Kwon SK, Park SY. Photopatterned arrays of fluorescent organic nanoparticles. Angew Chem Int Ed. 2007;46:1978–82.
6. Shi YL, Zhuo MP, Wang XD, Liao LS. Two-dimensional organic semiconductor crystals for photonics applications. ACS Appl Nano Mater. 2020;3:1080–97.
7. Collet E, Lemee-Cailleau MH, Buron-Le Cointe M, Cailleau H, Wulff M, Luty T, Koshihara SY, Meyer M, Toupet L, Rabiller P, Techert SM, Toupet L, Rabiller P, Techert S. Laser-induced ferroelectric structural order in an organic charge-transfer crystal. Science. 2003;300:612–5.
8. Zhao YS, Wu JS, Huang JX. Vertical organic nanowire arrays controlled synthesis and chemical sensors. J Am Chem Soc. 2009;131:3158–9.
9. Luo JD, Xie ZL, Lam JWY, Cheng L, Chen HY, Qiu CF, Kwok HS, Zhan XW, Liu YQ, Zhu DB, Tang BZ. Aggregation-induced emission of 1-methyl-1,2,3,4,5-pentaphenylsilole. Chem Commun. 2001:1740–1.
10. Lei YL, Jin Y, Zhou DY, Gu W, Shi XB, Liao LS, Lee ST. White-light emitting microtubes of mixed organic charge-transfer complexes. Adv Mater. 2012;24:5345–51.
11. Zhang YF, Peng C, Cui B, Wang ZF, Pang XB, Ma RM, Liu F, Che YK, Zhao JC. Direction-controlled light-driven movement of microribbons. Adv Mater. 2016;28:8538–45.
12. Bisri SZ, Piliego C, Gao J, Loi MA. Outlook and emerging semiconducting materials for ambipolar transistors. Adv Mater. 2014;26:1176–99.
13. Guo YL, Yu G, Liu YQ. Functional organic field-effect transistors. Adv Mater. 2010;22:4427–47.

14. Mas-Torrent M, Hadley P, Bromley S, Ribas X, Tarres J, Mas M, Molins E, Veciana J, Rovira C. Correlation between crystal structure and mobility in organic field-effect transistors based on single crystals of Tetrathiafulvalene derivatives. J Am Chem Soc. 2004;126:8546–53.
15. Kim J, Cho S, Kang J, Kim YH, Park SK. Large-scale organic single-crystal thin films and transistor arrays via the evaporation-controlled fluidic channel method. ACS Appl Mater Interfaces. 2014;6:7133–40.
16. Helfrich W, Schneider WG. Recombination radiation in Anthracene crystals. Phys Rev Lett. 1965;14:229–31.
17. Che Y, Yang X, Loser S, Zang L. Expedient vapor probing of organic amines using fluorescent Nanofibers fabricated from an n-type organic semiconductor. Nano Lett. 2008;8:2219–23.
18. Li ZZ, Liang F, Zhuo MP, Shi YL, Wang XD, Liao LS. White-emissive self-assembled organic microcrystals. Small. 2017;13:1604110.
19. Zheng JY, Zhang C, Zhao YS, Yao JN. Detection of chemical vapors with tunable emission of binary organic nanobelts. Phys Chem Chem Phys. 2010;12:12935–8.
20. Zhang HY, Zhang ZL, Ye KQ, Zhang JY, Wang Y. Organic crystals with tunable emission colors based on a single organic molecule and different molecular packing structures. Adv Mater. 2006;18:2369–72.
21. Chandrasekar R. Organic photonics: prospective nano/micro scale passive organic optical waveguides obtained from π-conjugated ligand molecules. Phys Chem Chem Phys. 2014;16:7173–83.
22. Venkatakrishnarao D, Mohiddon MA, Chandrasekhar N, Chandrasekar R. Photonic microrods composed of photoswitchable molecules: erasable heterostructure waveguides for tunable optical modulation. Adv Opt Mater. 2015;3:1035–40.
23. Chandrasekhar N, Mohiddon MA, Chandrasekar R. Organic submicro tubular optical waveguides: self-assembly, diverse geometries, efficiency, and remote sensing properties. Adv Opt Mater. 2013;1:305–11.
24. Hui P, Chandrasekar R. Light propagation in high-spin organic microtubes self-assembled from shape persistent macrocycles carrying oxo-verdazyl biradicals. Adv Mater. 2013;25:2963–7.
25. Basak S, Chandrasekar. Passive optical waveguiding organic rectangular tubes: tube cutting, controlling light propagation distance and multiple optical out-put. J Mater Chem C. 2014;2:1404.
26. Lin CCC, Chang PH, Su YW, Helmy AS. Monolithic Plasmonic Waveguide Architecture for Passive and Active Optical Circuits. Nano Lett. 2020;20:2950–7.
27. Annadhasan M, Agrawal AR, Bhunia S, Pradeep VV, Zade SS, Reddy CM, Chandrasekar R. Mechanophotonics: flexible single-crystal organic waveguides and circuits. Angew Chem Int Ed. 2020;59:13852–8.
28. Zhao GY, Dong HL, Liao Q, Jiang J, Luo Y, Fu HB, Hu WP. Organic field-effect optical waveguides. Nat Commun. 2018;9:4790–7.
29. Zhang C, Zheng JY, Zhao YS, Yao JN. Self-modulated white light outcoupling in doped organic nanowire waveguides via the fluctuations of singlet and triplet excitons during propagation. Adv Mater. 2011;23:1380–4.
30. Zheng JY, Yan YL, Wang XP, Zhao YS, Huang JX, Yao JN. Wire-on-wire growth of fluorescent organic heterojunctions. J Am Chem Soc. 2012;134:2880–3.
31. Zheng JY, Yan Y, Wang X, Shi W, Ma H, Zhao YS, Yao JN. Hydrogen peroxide vapor sensing with organic core/sheath nanowire optical waveguides. Adv Mater. 2012;24:OP194–9 OP86.
32. Zhuo MP, Wu JJ, Wang XD, Tao YC, Yuan Y, Liao LS. Hierarchical self-assembly of organic heterostructure nanowires. Nat Commun. 2019;10:3839.
33. Bao QL, Goh BM, Yan B, Yu T, Shen ZA, Loh KP. Polarized emission and optical waveguide in crystalline perylene diimide microwires. Adv Mater. 2010;22:3661–6.
34. Li Q, Jia Y, Dai LR, Yang Y, Li JB. Controlled rod nanostructured assembly of Diphenylalanine and their optical waveguide properties. ACS Nano. 2015;9:2689–95.
35. Cui QH, Peng Q, Luo Y, Jiang YQ, Yan YL, Wei C, Shuai ZG, Sun C, Yao JN, Zhao YS. Asymmetric photon transport in organic semiconductor nanowires through electrically controlled exciton diffusion. Sci Adv. 2018;4:eaap9861.
36. Wei GQ, Tao YC, Wu JJ, Li ZZ, Zhuo MP, Wang XD, Liao LS. Low-threshold organic lasers based on single-crystalline microribbons of aggregation-induced emission Luminogens. J Phys Chem Lett. 2019;10:679–84.
37. Hayashi S, Yamamoto SY, Takeuchi D, Ie Y, Takagi K. Creating Elastic Organic Crystals of π-Conjugated Molecules with Bending Mechanofluorochromism and Flexible Optical Waveguide. Angew Chem Int Ed. 2018;57:17002–8.
38. Liu HP, Lu ZQ, Zhang ZL, Wang Y, Zhang HY. Highly elastic organic crystals for flexible optical waveguides. Angew Chem Int Ed. 2018;57:8448.
39. Pradeep VV, Tardío C, Torres-Moya I, Rodríguez AM, Kumar AV, Annadhasan M, Hoz ADL, Prieto P, Chandrasekar R. Mechanical processing of naturally bent organic crystalline microoptical waveguides and junctions. Small. 2020;17:2006795.
40. Zhao YS, Xu JJ, Peng AD, Fu HB, Ma Y, Jiang L, Yao JN. Optical waveguide based on crystalline organic microtubes and microrods. Angew Chem Int Ed. 2008;47:7301–5.
41. Seok Min Yoon JL, Je JH, Choi HC, Yoon M. Optical Waveguiding and lasing action in Porphyrin rectangular microtube with Subwavelength Wall thicknesses. ACS Nano. 2011;5:2923–7.
42. Zhuo MP, Tao YC, Wang XD, Chen S, Liao LS. Rational synthesis of organic single-crystalline microrods and microtubes for efficient optical waveguides. J Mater Chem C. 2018;6:9594–8.
43. Liao Q, Fu HB, Yao JN. Waveguide modulator by energy remote relay from binary organic crystalline microtubes. Adv Mater. 2009;21:4153–7.
44. Zhuo MP, Fei XY, Tao YC, Fan J, Wang XD, Xie WF, Liao LS. In situ construction of one-dimensional component-interchange organic Core/Shell microrods for multicolor continuous-variable optical waveguide. ACS Appl Mater Interfaces. 2019;11:5298–305.
45. Li ZZ, Wu JJ, Wang XD, Wang KL, Zhang S, Xie WF, Liao LS. Controllable fabrication of in-series organic Heterostructures for optical waveguide application. Adv Opt Mater. 2019;7:1900373.
46. Sun MJ, Liu YY, Yan YM, Li R, Shi Q, Zhao YS, Zhong YW, Yao JN. In situ visualization of assembly and photonic signal processing in a triplet light-harvesting Nanosystem. J Am Chem Soc. 2018;140:4269–78.
47. Kong QH, Liao Q, Xu ZZ, Wang XD, Yao JN, Fu HB. Epitaxial self-assembly of binary molecular components into branched nanowire heterostructures for photonic applications. J Am Chem Soc. 2014;136:2382–8.

48. Li ZZ, Tao YC, Wang XD, Liao LS. Organic Nanophotonics: self-assembled single-crystalline homo−/Heterostructures for optical waveguides. ACS Photo. 2018;5:3763–71.
49. Min S, Dhamsaniya A, Zhang L, Hou G, Huang Z, Pambhar K, Shah AK, Mehta VP, Liu Z, Song B. Scale effect of a fluorescent waveguide in organic micromaterials: a case study based on Coumarin microfibers. J Phys Chem Lett. 2019; 10:5997–6002.
50. Yan YL, Zhao YS. Exciton Polaritons in 1D organic Nanocrystals. Adv Funct Mater. 2012;22:1330–2.
51. Zhang C, Zou CL, Yan Y, Hao R, Sun FW, Han ZF, Zhao YS, Yao JN. Two-photon pumped lasing in single-crystal organic nanowire Exciton Polariton resonators. J Am Chem Soc. 2011;133:7276–9.
52. Andreani L, Panzarini G, Gerard J. Strong-coupling regime for quantum boxes in pillar microcavities theory. Phys Rev B. 1999;60:13276–9.
53. Pile D, Forrest S. Organic polariton laser. Nat Photonics. 2010;4:402.
54. Takazawa K, Inoue J, Mitsuishi K, Takamasu T. Fraction of a millimeter propagation of exciton polaritons in photoexcited nanofibers of organic dye. Phys Rev Lett. 2010;105:067401.
55. Takazawa K, Inoue J, Mitsuishi K, Takamasu T. Micrometer-scale photonic circuit components based on propagation of exciton polaritons in organic dye nanofibers. Adv Mater. 2011;23:3659–63.
56. van Vugt LK, Ruhle S, Ravindran P, Gerritsen HC, Kuipers L, Vanmaekelbergh D. Exciton polaritons confined in a ZnO nanowire cavity. Phys Rev Lett. 2006;97:147401.
57. Zhao YS, Zhan P, Kim JY, Sun C, Huang JX. Patterned growth of vertically aligned. ACS Nano. 2010;4:1630–6.
58. Wang JF, Gudiksen MS, Duan XF, Cui Y, Lieber CM. Highly polarized photoluminescence and photodetection from single indium phosphide nanowires. Science. 2001;293:1455–7.
59. Wang ZL. Nanobelts, nanowires, and Nanodiskettes of semiconducting oxides-from materials to Nanodevices. Adv Mater. 2003;15:432–6.
60. Kind H, Yan HQ, Messer B, Law M, Yang PD. Nanowire ultraviolet Photodetectors and optical switches. Adv Mater. 2002; 14:158–3.
61. Wang XD, Liao Q, Kong QH, Zhang Y, Xu ZZ, Lu XM, Fu HB. Whispering-gallery-mode microlaser based on self-assembled organic single-crystalline hexagonal microdisks. Angew Chem Int Ed. 2014;53:5863–7.
62. Wang XD, Li H, Wu YS, Xu ZZ, Fu HB. Tunable morphology of the self-assembled organic microcrystals for the efficient laser optical resonator by molecular modulation. J Am Chem Soc. 2014;136:16602–8.
63. Wang XD, Liao Q, Li H, Bai SM, Wu YS, Lu XM, Hu HY, Shi Q, Fu HB. Near-infrared lasing from small-molecule organic hemispheres. J Am Chem Soc. 2015;137:9289–95.
64. Briseno AL, Mannsfeld SCB, Ling MM, Liu SH, Tseng RJ, Reese C, Roberts ME, Yang Y, Wudl F, Bao ZN. Patterning organic single-crystal transistor arrays. Nature. 2006;444:913–7.
65. Bisri SZ, Takenobu T, Yomogida Y, Shimotani H, Yamao T, Hotta S, Iwasa Y. High mobility and luminescent efficiency in organic single-crystal light-emitting transistors. Adv Funct Mater. 2009;19:1728–35.
66. Hotta S, Yamao T, Bisri SZ, Takenobu T, Iwasa Y. Organic single-crystal light-emitting field-effect transistors. J Mater Chem C. 2014;2:965–80.
67. Zhu WG, Zheng RH, Fu XL, Fu HB, Shi Q, Zhen YG, Dong HL, Hu WP. Revealing the charge-transfer interactions in self-assembled organic cocrystals: two-dimensional photonic applications. Angew Chem Int Ed. 2015;54:6785–9.
68. Yu PP, Zhen YG, Dong HL, Hu WP. Crystal engineering of organic optoelectronic materials. Chem. 2019;5:2814–53.
69. Yan B, Liao L, You YM, Xu XJ, Zheng Z, Shen ZX, Ma J, Tong LM, Yu T. Single-crystalline V_2O_5 ultralong nanoribbon waveguides. Adv Mater. 2009;21:2436–40.
70. Sun FF, Sun LX, Zhang B, Chen G, Wang HL, Shen XC, Wei L. Optical waveguide of buckled CdS nanowires modulated by strain engineering. ACS Photo. 2018;5:746–51.
71. Jadhav T, Dhokale B, Patil Y, Mobin SM, Misra R. Multi-stimuli responsive donor–acceptor Tetraphenylethylene substituted Benzothiadiazoles. J Phys Chem C. 2016;120:24030–40.
72. Yao W, Yan YL, Xue L, Zhang C, Li GP, Zheng QD, Zhao YS, Jiang H, Yao JN. Controlling the structures and photonic properties of organic nanomaterials by molecular design. Angew Chem Int Ed. 2013;52:8713–7.
73. Zhang C, Yan YL, Zhao YS, Yao JN. From molecular design and materials construction to organic nanophotonic devices. Acc Chem Res. 2014;47:3448–58.
74. Mitetelo N, Venkatakrishnarao D, Ravi J, Popov M, Mamonov E, Murzina TV, Chandrasekar R. Chirality-controlled multiphoton luminescence and second-harmonic generation from Enantiomeric organic micro-optical waveguides. Adv Opt Mater. 2019;7:1801775–6.
75. High AA, Novitskaya EE, Butov LV, Hanson M, Gossard AC. Control of exciton fluxes in an excitonic integrated circuit. Science. 2008;321:229–31.
76. Davoyan A, Engheta N. Electrically controlled one-way photon flow in plasmonic nanostructures. Nat Commun. 2014;5:5250.
77. Xu Q, Schmidt B, Pradhan S, Lipson M. Micrometre-scale silicon electro-optic modulator. Nature. 2005;435:325–7.
78. Hu WL, Chen YK, Jiang H, Li J, Zou JG, Zhang QJ, Zhang DG, Wang P, Ming H. Optical waveguide based on a polarized polydiacetylene microtube. Adv Mater. 2014;26:3136–41.
79. Yan Y, Zhang C, Zheng JY, Yao JN, Zhao YS. Optical modulation based on direct photon-plasmon coupling in organic/metal nanowire heterojunctions. Adv Mater. 2012;24:5681–6.
80. Liu Y, Hu HP, Xu L, Qiu B, Liang J, Ding F, Wang K, Chu MM, Zhang W, Ma M, Chen B, Yang XZ, Zhao YS. Orientation-controlled 2D anisotropic and isotropic photon transport in co-crystal polymorph microplates. Angew Chem Int Ed. 2020;59:4456–63.
81. Tang B, Zhang ZL, Liu HP, Zhang HY. Amplified spontaneous emission, optical waveguide and polarized emission based on 2,5-diaminoterephthalates. Chin Chem Lett. 2017;28:2129–32.
82. Ghosh S, Reddy CM. Elastic and bendable caffeine cocrystals: implications for the design of flexible organic materials. Angew Chem Int Ed. 2012;51:10319–23.
83. Ghosh S, Mishra MK, Kadambi SB, Ramamurty U, Desiraju GR. Designing elastic organic crystals: highly flexible polyhalogenated N-benzylideneanilines. Angew Chem Int Ed. 2015;54:2674–8.

84. Catalano L, Karothu DP, Schramm S, Ahmed E, Rezgui R, Barber TJ, Famulari A, Naumov P. Dual-mode light transduction through a plastically bendable organic crystal as an optical waveguide. Angew Chem Int Ed. 2018; 57:17254–8.
85. Annadhasan M, Karothu DP, Chinnasamy R, Catalano L, Ahmed E, Ghosh S, Naumov P, Chandrasekar R. Micromanipulation of mechanically compliant organic single-Crystal Optical microwaveguides. Angew Chem Int Ed. 2020;59:13821–30.
86. Zhu L, Al-Kaysi RO, Bardeen CJ. Reversible photoinduced twisting of molecular crystal microribbons. J Am Chem Soc. 2011;133:12569–75.
87. Saha S, Desiraju GR. Crystal engineering of hand-twisted helical crystals. J Am Chem Soc. 2017;139:1975–83.
88. Zhuo MP, Zhang YX, Li ZZ, Shi YL, Wang XD, Liao LS. Controlled synthesis of organic single-crystalline nanowires via the synergy approach of the bottom-up/top-down processes. Nanoscale. 2018;10:5140–7.
89. Fang XY, Yang XG, Yan DP. Vapor-phase π-π molecular recognition: a fast and solvent-free strategy towards the formation of co-crystalline hollow microtube with 1D optical waveguide and up-conversion emission. J Mater Chem C. 2017;5:1632–7.
90. Venkataramudu U, Venkatakrishnarao D, Chandrasekhar N, Mohiddon MA, Chandrasekar R. Single-particle to single-particle transformation of an active type organic μ-tubular homo-structure photonic resonator into a passive type hetero-structure resonator. Phys Chem Chem Phys. 2016;18:15528–33.
91. Sun YQ, Lei YL, Liao LS, Hu WP. Competition between Arene-Perfluoroarene and charge-transfer interactions in organic light-harvesting systems. Angew Chem Int Ed. 2017;56:10352–6.
92. Sun YQ, Lei YL, Sun XH, Lee ST, Liao LS. Charge-transfer emission of mixed organic Cocrystal microtubes over the whole composition range. Chem Mater. 2015;27:1157–63.
93. Xia HY, Chen YK, Yang G, Zou G, Zhang QJ, Zhang DG, Wang P, Ming H. Optical modulation of waveguiding in spiropyran-functionalized polydiacetylene microtube. ACS Appl Mater Interfaces. 2014;6:15466–71.
94. Zhou ZH, Zhao JY, Du YX, Wang K, Liang J, Yan YL, Zhao YS. Organic printed Core-Shell Heterostructure arrays: a universal approach to all-color laser display panels. Angew Chem Int Ed. 2020;59:11814–8.
95. Joo SH, Park JY, Tsung CK, Yamada Y, Yang P, Somorjai GA. Thermally stable Pt/mesoporous silica core-shell nanocatalysts for high-temperature reactions. Nat Mater. 2009;8:126–31.
96. Jang J, Oh JH. Facile fabrication of photochromic dye–conducting polymer Core–Shell Nanomaterials and their photoluminescence. Adv Mater. 2003;15:977–80.
97. Cui QH, Jiang L, Zhang C, Zhao YS, Hu WP, Yao JN. Coaxial organic p-n heterojunction nanowire arrays: one-step synthesis and photoelectric properties. Adv Mater. 2012;24:2332–6.
98. Pan DC, Wang Q, Jiang SC, Ji XL, An LJ. Synthesis of extremely small CdSe and highly luminescent CdSe/CdS Core-Shell Nanocrystals via a novel two-phase thermal approach. Adv Mater. 2005;17:176–4.
99. Mahler B, Nadal B, Bouet C, Patriarche G, Dubertret B. Core/shell colloidal semiconductor nanoplatelets. J Am Chem Soc. 2012;134:18591–8.
100. Zhu WG, Zhu LY, Zou Y, Wu YS, Zhen YG, Dong HL, Fu HB, Wei ZX, Shi Q, Hu WP. Deepening insights of charge transfer and Photophysics in a novel donor-acceptor Cocrystal for waveguide couplers and photonic logic computation. Adv Mater. 2016;28:5954–62.
101. Lei YL, Liao Q, Fu HB, Jao JN. Orange-blue-Orange Triblock one-dimensional Heterostructures of organic microrods for white-light emission. J Am Chem Soc. 2010;132:1742.
102. Ye X, Liu Y, Guo Q, Han Q, Ge C, Cui S, Zhang L, Tao XT. 1D versus 2D cocrystals growth via microspacing in-air sublimation. Nat Commun. 2019;10:761.
103. Zhang C, Yan YL, Jing YY, Shi Q, Zhao YS, Yao JN. One-dimensional organic photonic heterostructures: rational construction and spatial engineering of excitonic emission. Adv Mater. 2012;24:1703–8.
104. Zhang C, Yan Y, Yao JN, Zhao YS. Manipulation of light flows in organic color-graded microstructures towards integrated photonic heterojunction devices. Adv Mater. 2013;25:2854–9.
105. Yang C, Gu L, Ma C, Gu M, Xie X, Shi H, Ma H, Yao W, An Z, Huang W. Controllable co-assembly of organic micro/nano heterostructures from fluorescent and phosphorescent molecules for dual anti-counterfeiting. Mater Horiz. 2019;6:984–9.
106. Tao YC, Peng S, Wang XD, Li ZZ, Zhang XJ, Liao LS. Sequential self-assembly of 1D branched organic Homostructures with optical logic gate function. Adv Funct Mater. 2018;28:1804915.
107. Zhang Y, Liao Q, Wang XG, Yao JN, Fu HB. Lattice-matched epitaxial growth of organic Heterostructures for integrated optoelectronic application. Angew Chem Int Ed. 2017;56:3616–20.
108. Fang YR, Li ZP, Huang YZ, Zhang SP, Nordlander P, Halas NJ, Xu HX. Branched silver nanowires as controllable plasmon routers. Nano Lett. 2010;10:1950–4.
109. Yao W, Han GC, Huang F, Chu MM, Peng Q, Hu FQ, Yi YP, Jiang H, Yao JN, Zhao YS. "H"-like organic nanowire Heterojunctions constructed from cooperative molecular assembly for photonic applications. Adv Sci. 2015;2:1500130.
110. Yu Y, Tao YC, Zou SN, Li ZZ, Yan CC, Zhuo MP, Wang XD, Liao LS. Organic heterostructures composed of one- and two-dimensional polymorphs for photonic applications. Sci China Chem. 2020;63:1477–82.

Publisher's Note